PCCP

Accepted Manuscript

This is an *Accepted Manuscript*, which has been through the Royal Society of Chemistry peer review process and has been accepted for publication.

Accepted Manuscripts are published online shortly after acceptance, before technical editing, formatting and proof reading. Using this free service, authors can make their results available to the community, in citable form, before we publish the edited article. We will replace this *Accepted Manuscript* with the edited and formatted *Advance Article* as soon as it is available.

You can find more information about *Accepted Manuscripts* in the Information for Authors.

Please note that technical editing may introduce minor changes to the text and/or graphics, which may alter content. The journal's standard Terms & Conditions and the Ethical guidelines still apply. In no event shall the Royal Society of Chemistry be held responsible for any errors or omissions in this *Accepted Manuscript* or any consequences arising from the use of any information it contains.

ROYAL SOCIETY OF CHEMISTRY

www.rsc.org/pccp

Tungsten doped titanium dioxide nanowires for high efficiency dye-sensitized solar cells

P. S. Archana,[1] Arunava Gupta,[1] Mashitah M. Yusoff,[2] Rajan Jose[2*]

[1] Department of Chemistry, University of Alabama, 250 Hackberry Lane, Shelby hall, Tuscaloosa 35401, Alabama, USA; [2]Faculty of Industrial Sciences & Technology, Universiti Malaysia Pahang, 26300 Kuantan, Malaysia; * Corresponding author: E-mail: rjose@ump.edu.my

Abstract

Metal oxide semiconductors offering simultaneously high specific surface area and high electron mobility are actively sought for fabricating high performance nanoelectronic devices. The present study deals with synthesis of tungsten doped TiO_2 ($W:TiO_2$) nanowires (diameter ~ 50 nm) by electrospinning and evaluation of its performance in dye-sensitized solar cells (DSCs). Similarity in the ionic radii between W^{6+} and Ti^{4+} and availability of two free electrons per dopant are the rationale of the present study. Materials were characterized by X-ray diffraction, scanning and transmission electron microscopy, X-ray fluorescence measurements, and absorption spectroscopy. Nanowires containing 2 at.% $W:TiO_2$ gave 90% higher short circuit current density (J_{SC}) (~15.39 mA/cm^2) in DSCs with a nominal increase in the open circuit voltage compared with that of the undoped analogue (J_{SC} ~8.1 mA/cm^2). The results are validated by multiple techniques employing absorption spectroscopy, electrochemical impedance spectroscopy and open circuit voltage decay. The above studies show that the observed increments resulted from increased dye-loading, electron density, and electron lifetime in tungsten doped samples.

Physical Chemistry Chemical Physics Accepted Manuscript

Physical Chemistry Chemical Physics Accepted Manuscript

Keywords: Renewable Energy, Photovoltaics, Semiconductor Physics, Anatase, Organic-Inorganic Interface

1. Introduction

Modification of electrical properties of nanostructured metal oxide semiconductors (n-MOS), such as TiO_2, through appropriate doping is an active area of research in view of their potential applications in many electronic devices. The TiO_2, in particular, is a widely accepted material as a charge separation and transport medium in dye-sensitized solar cells, a renewable energy device in which the photovoltage appears at the junction between a dye-anchored n-MOS and a redox electrolyte.[1] Intense research during the past two decades brought the DSCs to a level of delivering a photovoltaic conversion efficiency (η)~12% in single cells[2] and ~9% in sub-modules[3] using mesoporous TiO_2 particles, inorganic dyes (porphyrin dyes, for example), and suitable electrolytes.

A number of studies are reported on doping TiO_2 either with a transition metal (Nb, Zr, Ni, Ta) for the Ti or an anion (N, F) for the O sites for improving its charge transport and electrochemical properties for fabricating high performance DSCs.[1,4-6] While both doping is beneficial in obtaining desired properties, transition metal doping offers additional advantages such as modified optical absorption, extended band edges, increased electron density of states and Fermi energy. Many dopants including, e.g., Nb, Zr, Ni, Ta, are doped in TiO_2 to favor modified absorption spectra, band edge energies, and electrical conductivity.[1,7] Among the transition metal dopants, optimal Nb doping produced a transparent conducting material which had higher optical transparency and electrical conductivity than the parent material.[8] The Nb doped TiO_2 (Nb:TiO_2) is shown to result in band edge type electron conduction in nanostructured

Physical Chemistry Chemical Physics Accepted Manuscript

TiO_2 owing to an increase in the Fermi level from the additional electron it gained per dopant when Nb^{5+} replaces Ti^{4+}.[9] Otherwise, the conduction is diffusive through their band gap in pure nanostructured semiconductors with an electron diffusivity lowered by several orders of magnitude.[10] However, the ionic radius of Nb^{5+} (0.64 Å) is ~6% higher than that of Ti^{4+} (0.605 Å) for six-fold coordination present in anatase;[11] thereby resulting in lattice strain in $Nb:TiO_2$. This lattice strain contributes to charge recombination; and thereby lowering the fill factor when the $Nb:TiO_2$ was used as photoelectrode in DSCs.[12,13] In other words, benefits of higher optical transparency and electrical conductivity achieved through Nb doping in TiO_2 is shadowed by strain in the lattice that contributes to electron loss in typical devices.

In this paper, we show that tungsten (W) doping in TiO_2 overcome these problems. Tungsten is preferred over niobium as a dopant for TiO_2 at least for two reasons, viz., (i) difference in the ionic radii (<0.005%) between W^{6+} (0.60 Å) and Ti^{4+} (0.605 Å) for six-fold coordination is negligible; and (ii) the W^{6+} doping for Ti^{4+} donates two free electrons/dopant compared with one free electron/dopant when Nb^{5+} replaces Ti^{4+}. Availability of two electrons is expected to further increase the Fermi level and would lead to enhanced performance in DSCs. In a previous work, Zhang et al[14] demonstrated increase in η and short circuit current density (J_{SC}) up to 20% using $W:TiO_2$ nanoparticles in DSCs. However, nanowires are preferred over nanoparticles in DSCs for several reasons including: (i) they offer directed electron channels and (ii) they can support a macroscopic electric field which would increase the J_{SC}. We have now developed nanowires of TiO_2 and $W:TiO_2$ and observed significantly more improved performance that has been achieved before. Our results show that, in addition to the increased electron lifetime (τ_n) reported by Zhang et al,[14] increased dye-loading on account of lowering of particle size forming the nanowires also contributed to the improved performance.

2. Experimental Details

Samples for the present study were in the form of nanowires synthesized by electrospinning, a nanofabrication technique for synthesis of advanced materials with variable aspect ratio, morphology, crystallinity, and functionality.[15,16] The TiO_2 and the W:TiO_2 nanowires were prepared by a commercial electrospinning machine (Electroris, nanoLab, Malaysia) using a previously adopted procedure.[12] The amounts of Ti and W precursors required were calculated based on the number of atoms required for replacing a given number of Ti atoms by W atoms. In the present work, 1 and 2 at.% W were doped in the TiO_2. The precursor solution for electrospinning was prepared from polyvinyl acetate (PVAc, Mw 500,000), dimethyl formamide (DMF), titanium (IV) isopropoxide (TTIP), tungsten hexachloride (Sigma Aldrich, 99.9%) and acetic acid. A stock solution of 11.5wt.% PVAc in DMF was prepared. In a typical synthesis, PVAc solution (4.5 g) was mixed with TTIP (2 g). Amount of the tungsten chloride was 0.028 and 0.057 g for 1 and 2 at.% doping, respectively. A sol was prepared by the dropwise addition of 0.5 g of acetic acid to the above solution. The viscosity of the solution for electrospinning was measured with a rheometer (LVDV III Ultra, Brookfield Co., USA). The viscosity of the pure PVAc solution was ~310 centipoise (cP), which is consistent with the results published by Ding et al[17] using polymer of similar molecular weight. However, the addition of TTIP and acetic acid lowered the viscosity to be 200 cP. The resulting solution was stirred well and electrospun at 25 kV accelerating voltage and at 1 ml/hr flow rate. The polymeric wires containing Ti^{4+} and W^{6+} ions were collected on a grounded rotating drum placed ~10 cm below the spinneret. The samples were sintered in air at 500 ^{o}C for 1 h to remove PVAc and allow nucleation and growth of TiO_2 particles in the fiber structure. The morphology of the nanowires were examined by and transmission electron microscopy (TEM; JEOL 2010Fas,

Physical Chemistry Chemical Physics Accepted Manuscript

Physical Chemistry Chemical Physics Accepted Manuscript

Japan). Crystal structures of the nanofibers were examined by X-ray diffraction (XRD, Siemens D5005, Bruker, Germany) technique. Presence of W was confirmed by X-ray fluorescence measurements (EDX-720, Shimadzu) (See Supplementary Information). Particulate properties of the samples were studied using BET surface area measurements (Micromeritics, Tristar 3000, USA). The optical bandgap of the fibers were determined from the UV-Vis-NIR absorption spectroscopy (UV-3600, Shimadzu).

For fabrication of DSCs, the TiO_2 and W:TiO_2 wires were directly spun on FTO glass substrates (1.5 cm x 1 cm; 25 Ω/□, Asahi Glass Co. Ltd., Japan), duly spun coated with a thin layer (~100 nm) of TiO_2. Thickness of the films was controlled by placing the FTO for different durations of time. The as-deposited fibrous films were then annealed at 500 ^{o}C for 1 h. Area of the films were fixed at 0.50 cm^2 based on recent recommendations.[18] Thickness of the films and its surface uniformity were studied by surface profilometry (Alpha–Step IQ Surface Profiler). The films were homogeneous and have uniform thickness (~15 μm). The DSCs were prepared by soaking the sintered electrodes in a dye solution containing in a 1:1 volume mixture of acetonitrile and tert-butanol of a ruthenium-based dye [$RuL_2(NCS)_2$-$2H_2O$; L = 2, 2' –bipyridyl-4,4'-dicarboxylic acid (0.5 mM), N3, Solaronix)] for 24 h at room temperature. The dye-sensitized samples were then washed in ethanol to remove unanchored dye and dried in air. Devices were sealed using a 50 μm spacer. A Pt sputtered FTO glass was used as the counter electrode. The I_3/I^- electrolyte was injected to the spacer region through two previously developed micro-holes. Photocurrent measurements of the assembled DSCs were performed using a solar simulator (San Ei, Japan) at air mass 1.5 global (AM1.5G) condition. The level of standard irradiance (100 mW/cm^2) was set with a calibrated c-Si reference solar cell. To avoid stray-light effects, devices were properly masked to expose only the photoelectrode area. The I-V curves were obtained using a potentiostat (Autolab PGSTAT30, Eco Chemie B.V., The Netherlands). Charge transport through the device was studied by the open circuit voltage decay (OCVD) and electrochemical impedance spectroscopy (EIS) measurements. The OCVD data was obtained by closing the illumination source to the device and recording the fall of V_{OC} using the Autolab instrument (PGSTAT30). The EIS studies used the Autolab PGSTAT30 in the frequency range 100 kHz to 0.1 Hz in the dark at a potential of 0.7 V.

3. Results and Discussion

In the present study, diameter of the TiO_2 wires was controlled by reducing the precursor concentration following Li et al.[19] The wires were of diameter ~50 nm composing of polycrystalline grains of sizes in the 5 – 20 nm range (Figure1). TEM studies showed W doping hindered the grain growth similar to that observed for Nb doping;[12] the size of the grain composing the wires systematically decreased with W doping (Figure 1). The lower particle size in the W:TiO_2 would increase the specific surface area of the nanowires which is beneficial for light harvesting through improved dye–loading when they are used as photoelectrode in DSCs. The samples were predominantly anatase (XRD pattern in Figure 2); however, a small (~2%) rutile phase was observed upon the W doping. The peaks in the XRD pattern were broadened upon W doping indicating lowering of particle size; consistent with the TEM observations. The lowering of the particle size of the W:TiO_2 samples were displayed in the gas adsorption studies by an increase in specific surface area. The BET surface area of the pure TiO_2, 1at.%W:TiO_2, 2at.%W:TiO_2, were 24, 24, and 36 m^2/g, respectively, which corroborates the TEM and XRD results.

Physical Chemistry Chemical Physics Accepted Manuscript

Physical Chemistry Chemical Physics Accepted Manuscript

Figure 3 shows the absorption spectra of the pure and W doped TiO_2 nanowires. The band edge absorption blue shifted with W doping indicating widening of optical band gap upon doping. The widening of the band gap can be understood from the bonding characteristics of the orbitals forming the conduction band of TiO_2. In TiO_2, the conduction band is formed from the overlapping of Ti(3d) orbitals. The W(5d) orbitals, which are at higher energies than the Ti(3d), shifts the conduction band to higher energies than the undoped samples. Interestingly, an additional absorption band was observed in the 350 – 500 nm range, the intensity of which increased with increasing doping concentration. The broad absorption observed in W-doped samples could be assigned to $W^{6+}\leftrightarrow W^{5+}$; $W^{5+}\leftrightarrow W^{4+}$; and $W^{6+}\leftrightarrow W^{4+}$ transitions to accommodate the charge changes due to doping.[20]

Figure 4 shows the current density (J_{SC}) *vs*. voltage (V) plots for the best DSCs fabricated using TiO_2 and W:TiO_2 nanowires; summary of photovoltaic properties for measurements of four DSCs in each sets are in Table 1. Data for Nb:TiO_2 is also shown for comparison. Note that devices used in this work were similar to the one used in the landmark paper by O Regan and Grätzel, reporting 7% efficiency in DSCs, employing similar dye (N3) and electrolyte (iodide/triiodide).[21] Over the years, efficiency of DSCs enhanced to >12% using more efficient dyes, electrolytes, and light scattering electrode layers.[2] Requirement of high efficiencies in DSCs are (i) compact but porous electrode, (ii) highly purified dyes, (iii) choice of dyes and electrolytes, and (iv) presence of scattering layers to enhance light sensitivity.[22] The N3 dye and iodide/triiodide based electrolyte used in this experiments were as-received and without any further purification; therefore, the efficiencies in Table 1 are comparable to the state of the art devices. The 2at.%W:TiO_2 based devices showed 8% higher V_{OC} (882 mV), 90% higher J_{SC} (15 mA/cm^2), and 100% enhanced η (8.55%) compared to the undoped analogue. A nominal increase in fill factor (*FF*) by <1% was observed for the 2at.% W:TiO_2 compared with the undoped analogue; on the other hand, Nb doping result in drastic lowering of *FF* (>10%). Therefore, the main source of increase of the photoconversion efficiency is the observed 90% increase in J_{SC}, which can be originated from two sources viz. (i) higher dye-loading and (ii) its improved charge transport characteristics. Figure 5 shows the UV-Vis absorption spectra of the dye-anchored electrodes; no contribution in J_{SC} was evident from the additional absorption band observed upon W doping (Fig. 3). No additional light scattering was observed in W:TiO_2 electrodes, which is most likely because of the similarity in the diameters of the wires. The measured dye-loading was 30% higher for the 2at.%W:TiO_2 samples (~0.26 μmol/cm^2) compared to the undoped ones (~0.20 μmoles/cm^2). The lower-sized particles in W:TiO_2 enabled a higher dye-loading thereby masking additional light scattering compared with undoped analogue. An increase of dye-loading by 20% is reported to increase the J_{SC} by 30% and incident photon to current conversion efficiency (IPCE) by 3%;[23] therefore, assuming a linear relationship allowed by similarity in the light scattering, ~45% of the increase in J_{SC} of the 2at.%W:TiO_2 device is from the improved dye-loading. Given that $J = ne\sigma$, where n is the electron density, e is the elementary charge, and σ is the electrical conductivity, remaining 45% increase in J_{SC} is expected to result from increased electron density due to doping and electrical conductivity due to improved charge transport characteristics.

The variation in charge transport with respect to the area of the device was studied by EIS.[24] The electrical equivalent of DSCs comprises of resistors and capacitors representing various interfacial and transport processes in the device; the total impedance of such electrical equivalent is expressed as:

Physical Chemistry Chemical Physics Accepted Manuscript

$$Z(\omega) = 2\left(\frac{R_T}{R_{CT}}\right)^{1/2} \frac{1}{C_\mu}(i\omega_{CT})^{-\beta} \qquad (1)$$

where R_T is the total resistance offered by the photoelectrode, R_{CT} is the resistance to the charge transfer from the photoelectrode to the electrolyte, ω_{CT} is the characteristic frequency at which the charge transfer occurs, and the parameter β is the exponent of the constant phase element representing the deviation from capacitance at the planer semiconductor – electrolyte interface.[24] Figure 6(A) is a typical EIS spectrum of DSCs in which the above parameters are represented. The high frequency offset is the series resistance Rs of the cell originate primarily from the FTO resistance. The EIS spectrum of DSCs displays three semi circles which are assigned to three processes, viz., (i) resistance to the electron transport (R_T) through the electrode material occurs at high frequency (> 0.1 kHz); (ii) resistance to the charge recombination (R_{CT}) between the electrons in the electrode material and the redox species in the electrolyte occurs at intermediate frequencies (0.1 kHz $<f<$ 1 Hz); and resistance to ion diffusion occurs at lower frequencies (< 1 Hz).

Figure 6(B) shows the Nyquist plot of the 2at%W:TiO_2 compared with that of the pure TiO_2 and 2at%Nb:TiO_2 nanowires recorded at a typical bias voltage of 0.7 V. Data for 2at%Nb:TiO_2 is from our previous publication.[9] Both real (Z') and imaginary (Z'') parts of the total impedance as well as ω_{CT} increased in the order TiO_2<Nb:TiO_2< W:TiO_2 showing the crucial dependence of doping on charge transport. The R_T, which is evaluated from the x-intercept of a line drawn from the liner-onset of the second semicircle in the EIS spectrum,[25] is nearly constant at ~28±1 Ω, which could be attributed to the directional charge transport in nanowires. Therefore, the origin of higher J_{SC} in the W:TiO_2 is expected to arise from the charge

Physical Chemistry Chemical Physics Accepted Manuscript

transport dynamics determined by the electron lifetime (τ_n) and R_{CT}. The τ_n can be obtained from the Bode plots (Figure 6B) using the relation $\tau_n = 1/(2\pi f_c)$, where f_c is the peak frequency which for TiO_2, Nb:TiO_2, and W:TiO_2 were 3.75, 0.88, and 0.43 Hz at 0.7 V, respectively. These frequencies correspond to a τ_n of 42, 181, and 374 ms, respectively. i.e., electrons live much longer in the W:TiO_2 nanowires compared to the other two samples. Electrons with longer τ_n survive recombination; therefore, characterized by larger R_{CT}. A qualitative estimation of the R_{CT} could be obtained from mid-frequency region of the EIS spectrum (Bode plots in Figure 6D). The R_{CT} of the W:TiO_2 is higher than that of the Nb:TiO_2 thereby accounting the higher J_{SC} and FF of the tungsten doped samples. The R_{CT} calculated from the EIS curve employing Eq. (1) was 63, 176, 341 Ω.cm for TiO_2, Nb:TiO_2, and W:TiO_2, respectively. Therefore, due to longer τ_n and larger R_{CT} the devices fabricated using W:TiO_2 showed improved J_{SC} and FF than the TiO_2 and the Nb doped analogue.

Open circuit voltage decay (OCVD) measurements were carried out to validate the longer τ_n in the W:TiO_2 sample. The OCVD measures the temporal decay of V_{OC} upon removing the illumination source in a DSC operating at steady state thereby providing a real time measurement of charge transport through the device.[26] At V_{OC}, the psudo-Fermi level reaches the conduction band[10] which falls to its original level once the light absorption by the dye is terminated. i.e., when the light source is removed. Under steady state in DSCs, the electrons injected into the photoelectrode is equal to that removed from the contact electrode. When the electron injection is terminated by closing the light source, the electrons in the conduction band of TiO_2 decays until its Fermi level; consequently, the V_{OC} shows a delay before reaching zero, which is typically measured in the OCVD. Assuming a first order recombination reaction, the τ_n as a function of voltage is given by $\tau_n = -(kT/e)(dV_{OC}/dt)^{-1}$,[26,27] where kT is the thermal energy, e is the

Physical Chemistry Chemical Physics Accepted Manuscript

positive elementary charge and dV_{oc}/dt is the first order time derivative of the V_{OC}. Figure 7 compares the τ_n of the devices as a function of voltage determined from the OCVD curves. The τ_n of the W:TiO_2 is higher than the undoped analogue in the entire range of V_{OC}. For a typical decay voltage of 0.7 V, the τ_ns were 0.384, 0.502, and 1.2 s for TiO_2, 2 at.% Nb:TiO_2, 2 at.% W:TiO_2 nanowires, respectively. i.e., the τ_n of the 2 at.% W:TiO_2 marked over 100% increase compared to the undoped analogue similar to that observed from the EIS data.

The difference in τ_n between the samples could be related to the difference in the electron density achieved upon doping. Unlike that of bulk MOS, energy gap of n-MOS is not completely forbidden but characterized by a broad distribution of localized energy states[10,24,28] arise from the deviation of equilibrium atomic coordinates.[1,29] Density of those localized states is higher at the bottom of the conduction band and exponentially decreases in the energy scale towards the Fermi level. The photogenerated electrons in the n-MOS are trapped by the localized states and subsequent thermal activation leads the electrons to deeper energy levels and retrap again. The injected carriers thus move via a trap-detrap, otherwise called multiple trapping (MT), through the band gap.[28] On the other hand, electrons in the bulk semiconductors hop from one transport state to other in the conduction band. Therefore, τ_n in n-MOS is lower by several orders of magnitude than the corresponding bulk material. Arther Frank and others have reported a number of experiments using MOS nanotubes and nanowires that removal of structural disorders lead to increase in τ_n and other charge transport parameters.[30-35]

However, in case of W and Nb doping, the increase in τ_n was followed by an inferior crystallinity (Figure 1). We have recently shown by measuring chemical capacitance (C_μ) in Nb:TiO_2 that doping uplifts the Fermi level of MOS thereby supporting band edge type conduction.[9] The C_μ of a material represents the change in its electron density as a function of a

Physical Chemistry Chemical Physics Accepted Manuscript

Physical Chemistry Chemical Physics Accepted Manuscript

small variation in chemical potential induced by variations in morphology, crystal structure, degree of crystallinity, and doping.[36] The C_μ of the materials determined from the EIS spectra using the procedure outlined elsewhere[25] is 0.99, 1.21 and 1.68 mF/cm^2 at 0.7 V for TiO_2, Nb:TiO_2 and W:TiO_2, respectively. Considerable variation in electron density thus obtained uplifts the Fermi level of the W:TiO_2 compared with TiO_2 and result in band edge type conduction, as shown before, and result in improved τ_n.

In conclusion, we have shown that tungsten doping in TiO_2 is preferred over other dopants for their application as a photoelectrode in nanowire dye-sensitized solar cells. The results of our experiments show that tungsten doping (i) hindered the grain growth to have larger available surface and (ii) increased electron lifetime on account of increased electron density. A nominal doping of 2at.% tungsten in TiO_2 increases the short circuit current density of dye-sensitized solar cells by 90%. We have shown that the dye-loading increased by 30% that contributed ~45% increase in the short circuit current density. Our electrochemical impdedance spactroscopy and open circuit voltage decay experiments show a 100% increase in the electron lifetime in tungsten doped TiO_2, which is expected to be the source of remaining 45% increase in the short circuit current density. The tungsten doped TiO_2 is likely be an acceptable material for commercial dye-sensitized solar cells.

Acknowledgements

This work was financially supported by the Malaysian Technological University Network (MTUN) research grant on nanowire dye-sensitized solar cells (RDU 121210).

Supplementary Materials Available: Thermal analyses results of PVAc fiber containing the titanium precursor (S1), X-ray fluorescence spectrum of the tungsten doped samples (S2) and transmission electron micrographs, both bright field and lattice images, of the Nb-doped samples (S3). This material is available free of charge via the internet http://rsc.org.

Physical Chemistry Chemical Physics Accepted Manuscript

References

[1] R. Jose, V. Thavasi, and S. Ramakrishna, J. Am. Ceram. Soc. **92,** 289-301 (2009).

[2] A. Yella, H.-W. Lee, H. N. Tsao, C. Yi, A. K. Chandiran, M. K. Nazeeruddin, E. Wei-Guang Diau, C.-Y. Yeh, S. M. Zakeeruddin, and M. Grätzel, Science **334,** 629 (2011).

[3] S. Shrestha, Progress in Photovoltaics: Research and Applications **19,** 754-756 (2011).

[4] K. Lee and P. Schmuki, Electrochem. Commun. **25,** 11-14 (2012).

[5] V. Thavasi, V. Renugopalakrishnan, R. Jose, and S. Ramakrishna, Mater. Sci. Eng.: R: Reports **63,** 81-99 (2009).

[6] C. T. Cherian, M. V. Reddy, T. Magdaleno, C.-H. Sow, K. V. Ramanujachary, G. V. S. Rao, and B. V. R. Chowdari, CrystEngComm **14,** 978-986 (2012).

[7] P. S. Archana, E. Naveen Kumar, C. Vijila, S. Ramakrishna, M. M. Yusoff, and R. Jose, Dalton Trans. **42,** 1024-1032 (2013).

[8] F. Yutaka, H. Taro, Y. Yukio, I. Kazuhisa, K. Go, H. Yasushi, S. Toshihiro, and H. Tetsuya, Appl. Phys. Lett. **86,** 252101 (2005).

[9] P. S. Archana, R. Jose, M. M. Yusoff, and S. Ramakrishna, App. Phys. Lett. **98,** 152106 (2011).

[10] J. Bisquert, Phys Chem Chem Phys **10,** 49-72 (2008).

[11] R. D. Shannon, Acta. Cryst **A32,** 751-767 (1976).

[12] P. S. Archana, R. Jose, T. M. Jin, C. Vijila, M. M. Yusoff, and S. Ramakrishna, J. Am. Ceram. Soc. **93,** 4096-4102 (2010).

[13] X. J. Lu, X. L. Mou, J. J. Wu, D. W. Zhang, L. L. Zhang, F. Q. Huang, F. F. Xu, and S. M. Huang, Ad. Func. Mater. **20,** 509-515 (2010).

Physical Chemistry Chemical Physics Accepted Manuscript

[14] X. Zhang, F. Liu, Q. L. Huang, G. Zhou, and Z. S. Wang, J. Phys. Chem. C **115,** 12665-12671 (2011).

[15] S. Ramakrishna, R. Jose, P. S. Archana, A. S. Nair, R. Balamurugan, J. R. Venugopal, and W. E. Teo, J. Mater. Sci. **45,** 6283-6312 (2010).

[16] R. Ramasheshan, S. Sundarrajan, R. Jose, and S. Ramakrishna, J. Appl. Phys. **102,** 111101 (2007).

[17] B. Ding, H. Kim, C. Kim, M. Khil, and S. Park, Nanotechnol. **14,** 532-537 (2003).

[18] A. Fakharuddin, P. S. Archana, Z. Kalidin, M. M. Yusoff, and R. Jose, RSC Adv. **3,** 2683-2689 (2013).

[19] D. Li and Y. Xia, Nano Lett. **3,** 555-560 (2003).

[20] L. Berggren, J. C. Jonsson, and G. A. Niklasson, J. Appl. Phys. **102,** 083538 (2007).

[21] B. O'Regan and M. Grätzel, Nature **353,** 737-9 (1991).

[22] S. Ito, T. N. Murakami, P. Comte, P. Liska, C. Gratzel, M. K. Nazeeruddin, and M. Gratzel, Thin Solid Films **516,** 4613-4619 (2008).

[23] T. Ma, K. Inoue, K. Yao, H. Noma, T. Shuji, E. Abe, J. Yu, X. Wang, and B. Zhang, J. Electroanal. Chem. **537,** 31-38 (2002).

[24] J. Bisquert, F. Fabregat-Santiago, I. Mora-Seró, G. Garcia-Belmonte, E. M. Barea, and E. Palomares, Inor. Chimica Acta **361,** 684-698 (2008).

[25] J. Bisquert, G. Garcia-Belmonte, F. Fabregat-Santiago, N. S. Ferriols, P. Bogdanoff, and E. C. Pereira, J. Phys. Chem. B **104,** 2287-2298 (2000).

[26] A. Zaban, M. Greenshtein, and J. Bisquert, ChemPhysChem **4,** 859-864 (2003).

[27] J. Bisquert, A. Zaban, M. Greenshtein, and I. Mora-Sero, J. Am. Chem. Soc. **126,** 13550-13559 (2004).

Physical Chemistry Chemical Physics Accepted Manuscript

[28] J. Bisquert, J. Phys. Chem. C **111,** 17163-17168 (2007).

[29] R. Jose, N. U. Zhanpeisov, H. Fukumura, Y. Baba, and M. Ishikawa, J. Am. Chem. Soc. **128,** 629-636 (2006).

[30] P. S. Archana, R. Jose, C. Vijila, and S. Ramakrishna, J. Phys. Chem. C **113,** 21538-21542 (2009).

[31] K. Zhu, T. B. Vinzant, N. R. Neale, and A. J. Frank, Nano Lett. **7,** 3739-3746 (2007).

[32] K. Zhu, N. R. Neale, A. Miedaner, and A. J. Frank, Nano Lett. **7,** 69-74 (2007).

[33] N. Kopidakis, K. D. Benkstein, J. van de Lagemaat, A. J. Frank, Q. Yuan, and E. A. Schiff, Phys. Rev. B **73,** 045326 (2006).

[34] N. K. Elumalai, C. Vijila, R. Jose, K. Zhi Ming, A. Saha, and S. Ramakrishna, Phys Chem Chem Phys **15,** 19057-19064 (2013).

[35] N. K. Elumalai, A. Saha, C. Vijila, R. Jose, Z. Jie, and S. Ramakrishna, Phys Chem Chem Phys **15,** 6831-6841 (2013).

[36] J. Bisquert, Phys. Chem. Chem. Phys. **5,** 5360-5364 (2003).

Physical Chemistry Chemical Physics Accepted Manuscript

Table 1: Statistics of the photovoltaic parameters of the pure and tungsten doped TiO_2

Electrode	J_{SC} (mA/cm^2)		V_{OC} (V)		FF (%)		η (%)	
	Mean	Best	Mean	Best	Mean	Best	Mean	Best
TiO_2	7.8	8.1	0.803	0.815	66	67	4.14	4.17
1wt.% W: TiO_2	11.97	12.42	0.807	0.848	59.9	61	5.76	5.97
2wt.% W: TiO_2	15	15.39	0.878	0.882	66.1	66.3	8.71	8.99
2wt.% Nb: TiO_2	-	13.79	-	0.720	-	57	-	5.66

Physical Chemistry Chemical Physics Accepted Manuscript

Physical Chemistry Chemical Physics Accepted Manuscript

Figure Captions

Figure 1: Bright field TEM images of (a) pure TiO_2, (b) 1at.%W:TiO_2, (c) 2at.%W:TiO_2, and (d) a HRTEM image showing high porosity in the 2at.%W:TiO_2. Insets: selected area diffraction patterns of the (a) pure TiO_2 showing diffraction spots correspond to extended crystallinity and (b) & (c) tungsten doped samples indicating polycrystalline ring patterns.

Figure 2: XRD patterns of (a) pure TiO_2, (b) 1at.%W:TiO_2, (c) 2at.%W:TiO_2 and tungsten doped TiO_2. All the peaks except the one at $2\theta \sim 27.1^{o}$ are due to anatase.

Figure 3: UV-Vis absorption spectra of pure and tungsten doped TiO_2.

Figure 4: Current – voltage characteristics of the solar cells made using pure and tungsten doped TiO_2. An I-V curve of the Nb:TiO_2 is also added for comparison.

Figure 5: Absorption spectra of (a) N3 dye, (b) N3 dye-anchored TiO_2, and (c) N3 dye-anchored W:TiO_2 showing enhanced dye-loading. The spectrum of the pure dye was recorded in solution and the samples for the other two were films on glass substrate. i The amount of dye used for the measurement was 0. 38 μmol and comparison of the dye-loading between pure and tungsten doped TiO_2.

Figure 6: (a) EIS spectrum showing the three processes as explained in the text. The "W" stands for resistance to ion diffusion. Refer text for details. (b) Nyquist plot of doped and undoped samples (see figure labels); (c) Bode plots of doped and undoped samples showing phase angle (θ) as a function of frequency (see figure labels); (d) the total impedance in the mid frequency region indicating the recombination resistance.

Figure 7: The electron lifetime as a function of decay voltage derived from the open circuit voltage decay curves of pure and doped samples (See figure labels for details).

Physical Chemistry Chemical Physics Accepted Manuscript

Figure 1, Archana et al

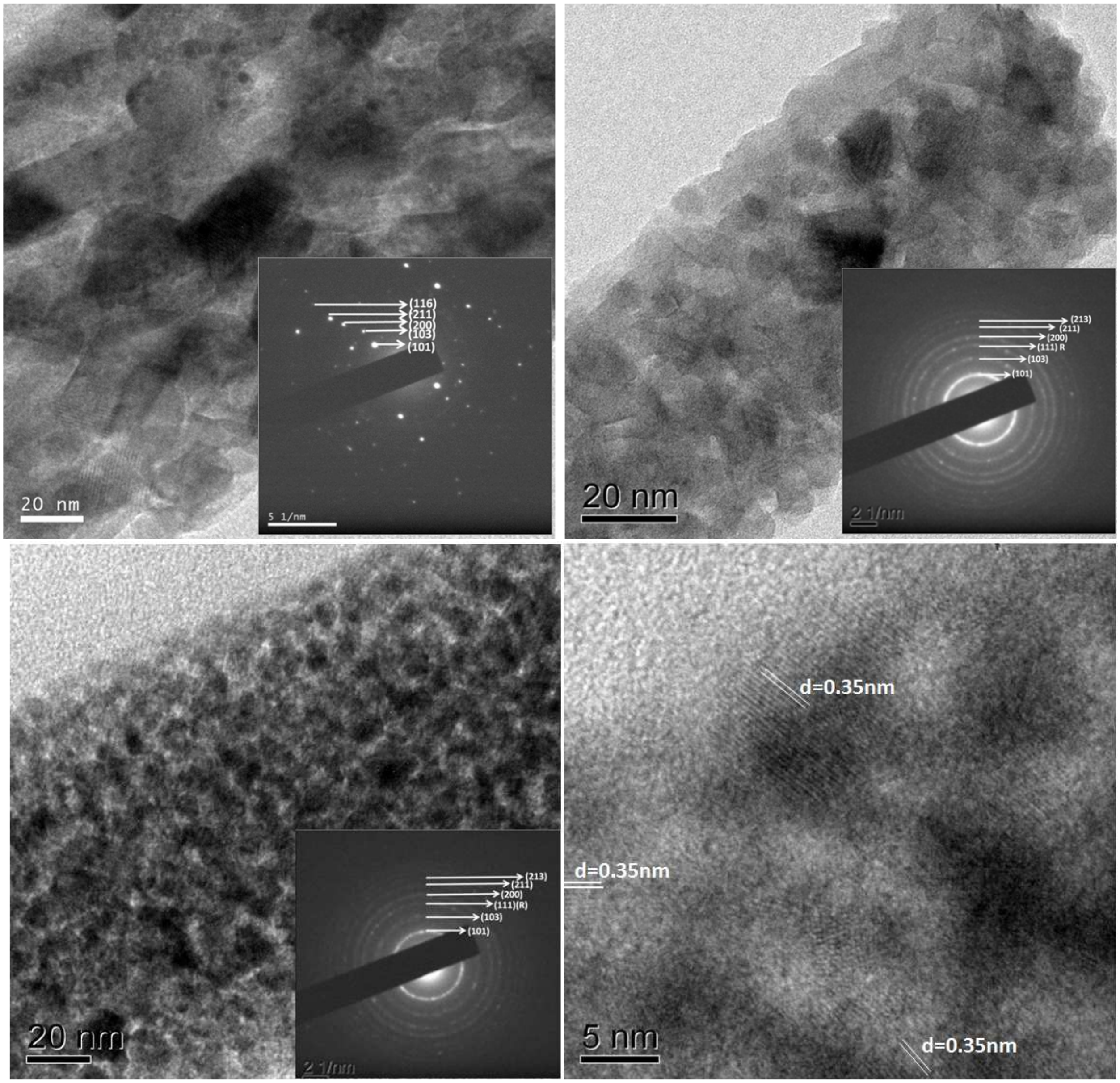

Physical Chemistry Chemical Physics Accepted Manuscript

Figure 2, Archana et al

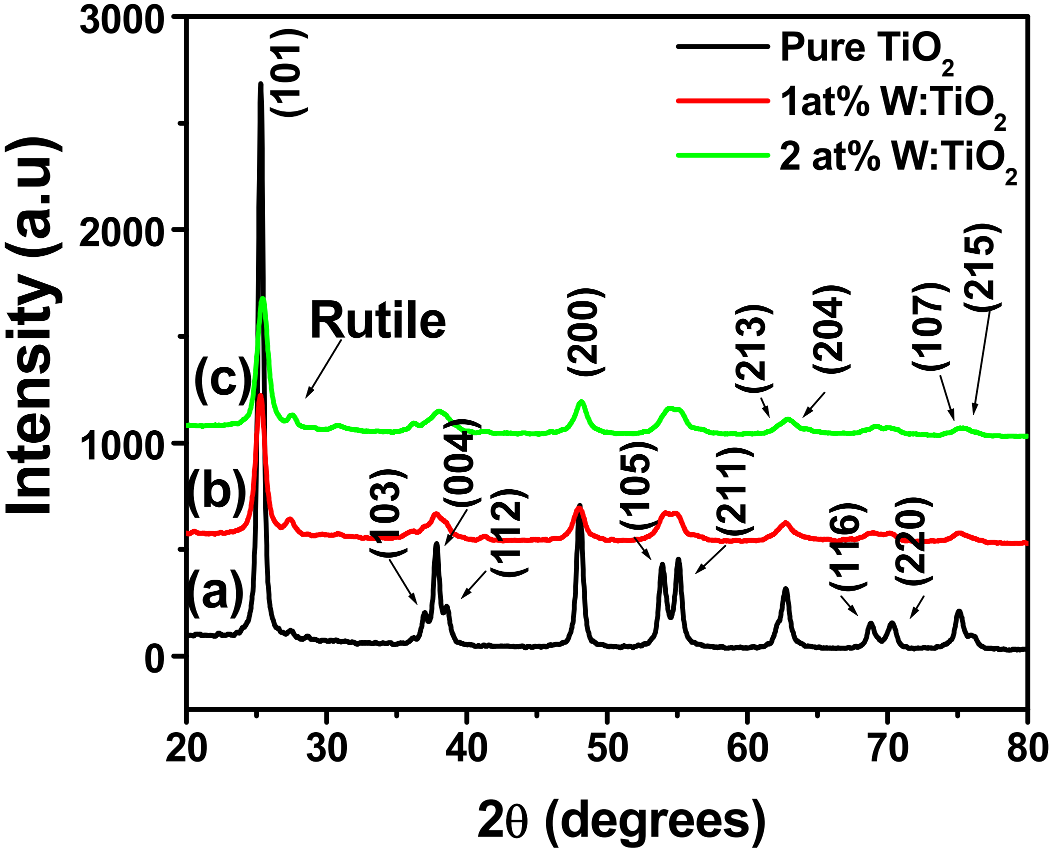

Physical Chemistry Chemical Physics Accepted Manuscript

Figure 3, Archana et al

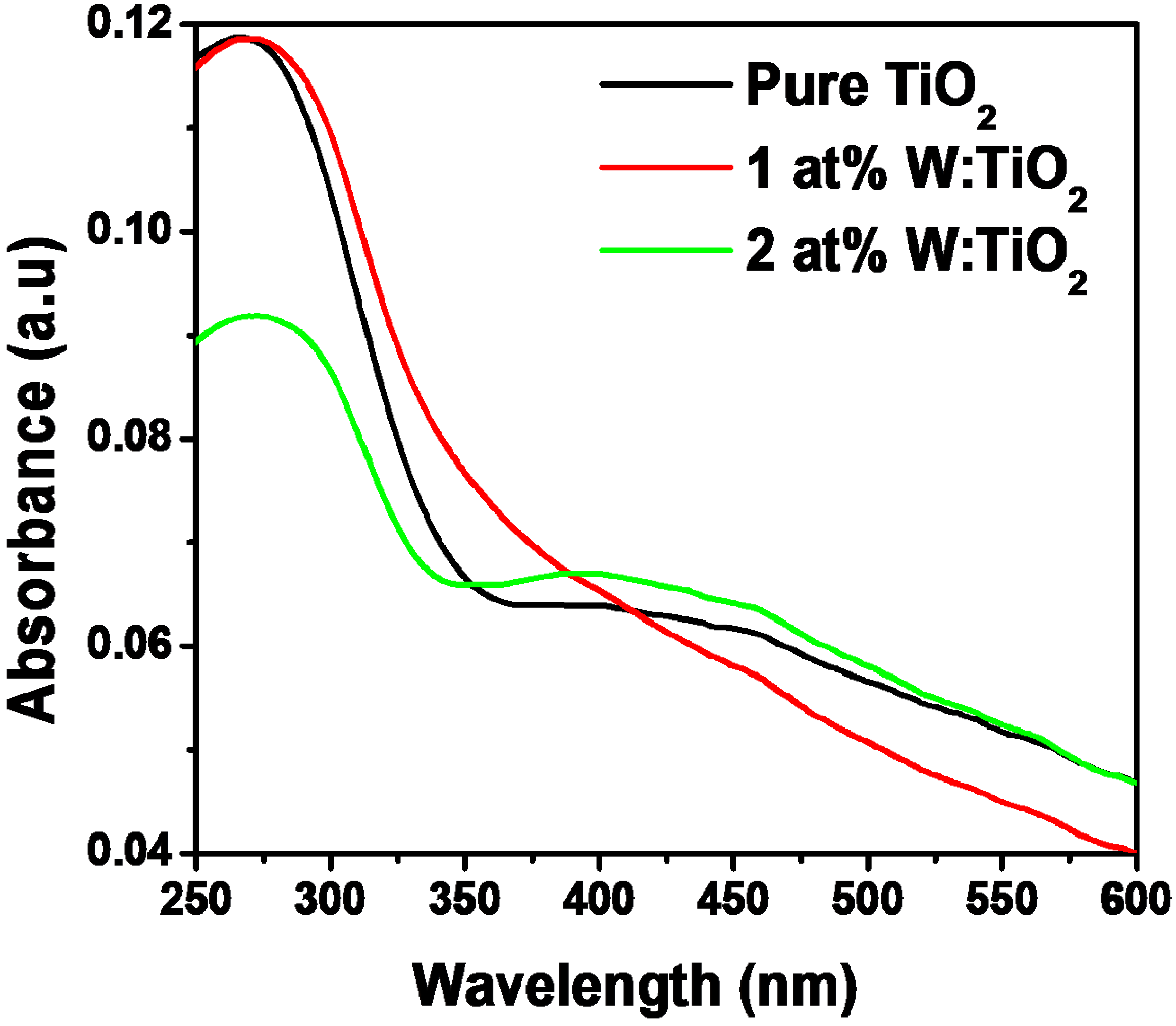

Physical Chemistry Chemical Physics Accepted Manuscript

Figure 4, Archana et al

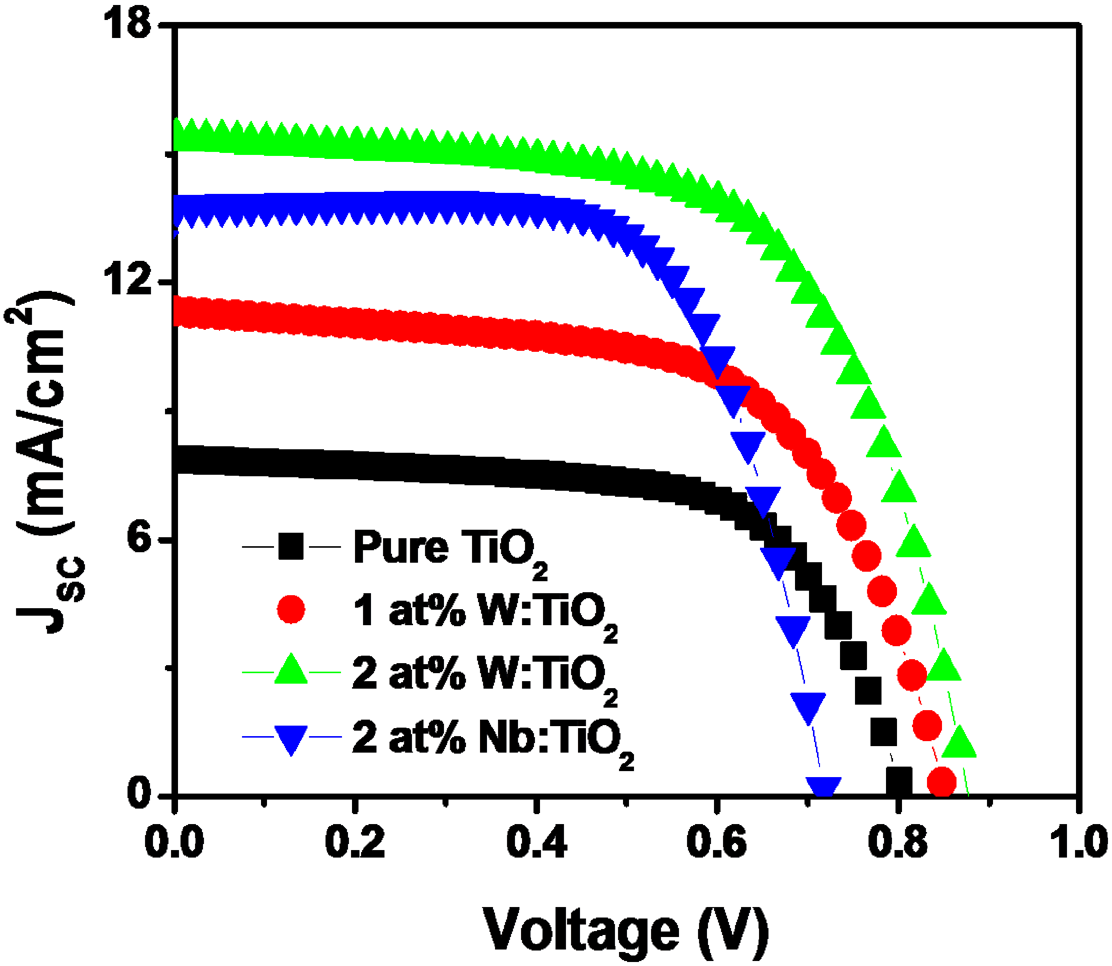

Physical Chemistry Chemical Physics Accepted Manuscript

Figure 5, Archana et al

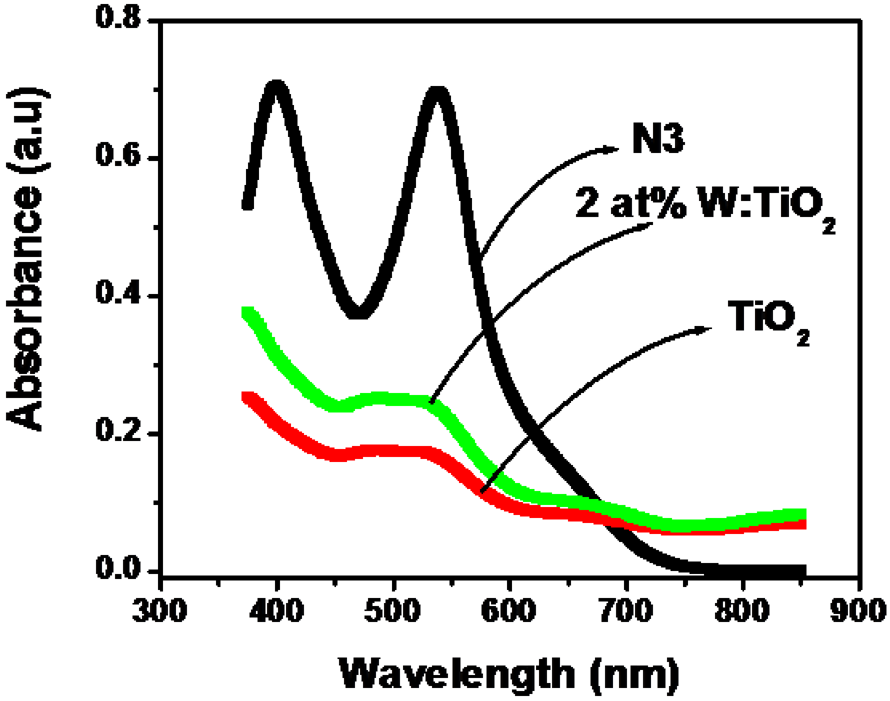

Physical Chemistry Chemical Physics Accepted Manuscript

Figure 6, Archana et al

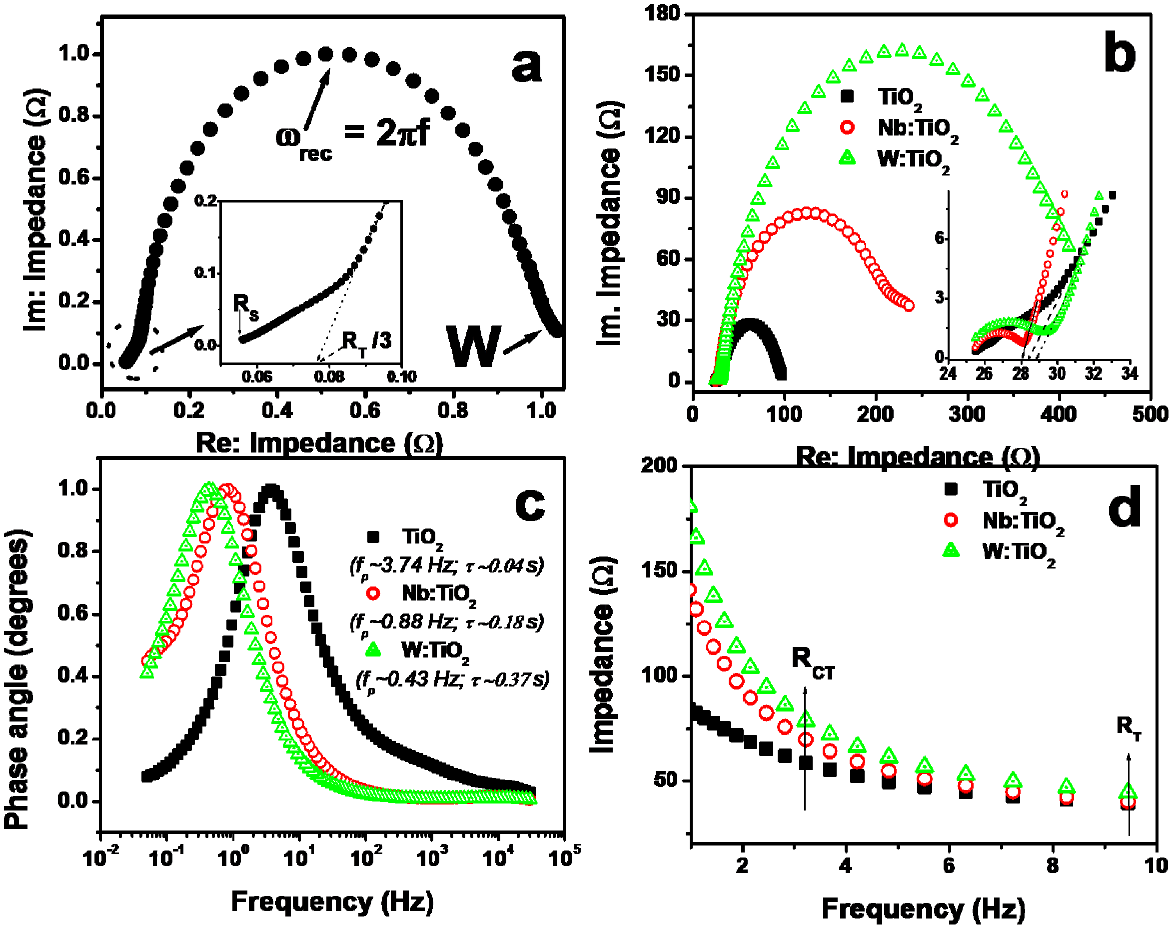

Physical Chemistry Chemical Physics Accepted Manuscript

Figure 7, Archana et al

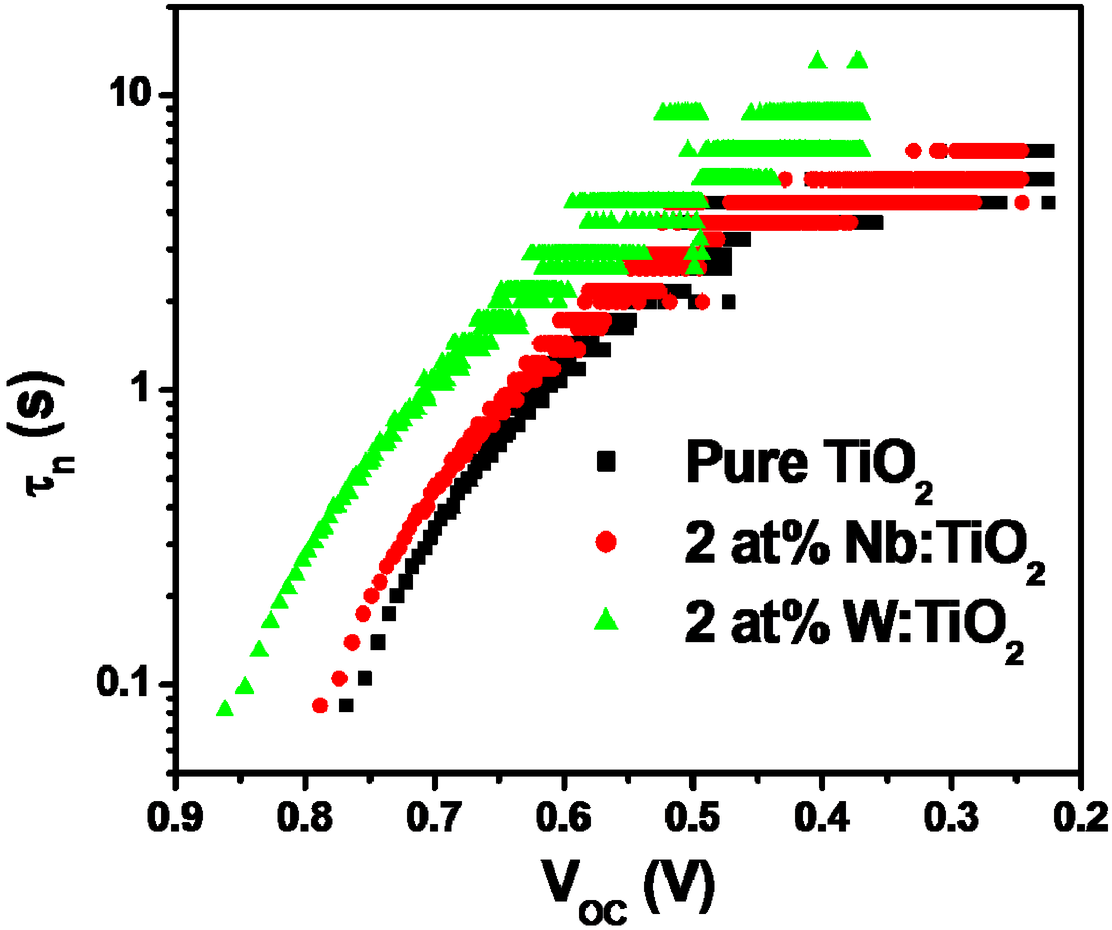

Physical Chemistry Chemical Physics Accepted Manuscript

Table of Content Entry

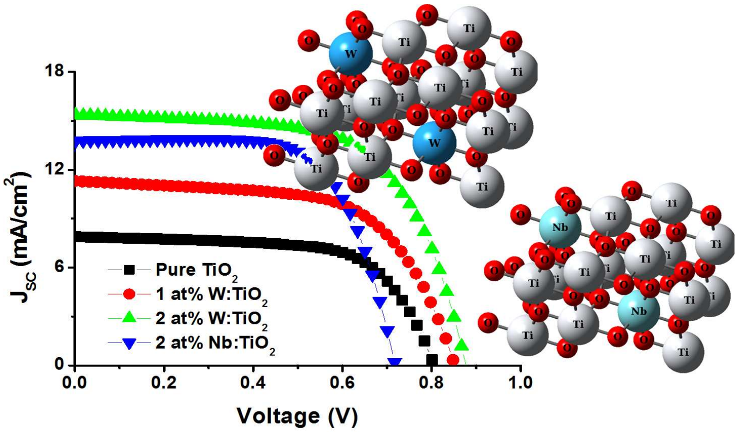

Tungsten doping in TiO_2 nanowires increases the photocurrent density from increased lifetime and dye-loading than niobium doping.

Physical Chemistry Chemical Physics Accepted Manuscript